Multiple skeletal and dental pathologies in a late Miocene mesotheriid (Mammalia, Notoungulata) from the Altiplano of Bolivia: Palaeoecological inferences

Marcos Fernandez-Monescillo, Pierre-Olivier Antoine, Bernardino Mamani Quispe, Philippe Munch, Rubén Andradre Flores, Laurent Marivaux, Francois Pujos

Multiple skeletal and dental palaeopathologies in a mesotheriid individual (Mammalia, Notoungulata) and palaeoecological inferences in the upper Miocene of the Bolivian Altiplano.

Marcos Fernández-Monescillo [a,*],Pierre-Olivier Antoine [b],Bernardino Mamani Quispe [c], Philippe Münch [d],Rubén Andrade Flores [c],Laurent Marivaux [b], François Pujos [a]

[a] *Instituto Argentino de Nivología, Glaciología y Ciencias Ambientales (IANIGLA), CCT–CONICET–Mendoza, Avda. Ruíz Leal s/n, Parque Gral. San Martín, 5500 Mendoza, Argentina*

[b] *Institut des Sciences de l'Evolution, cc64, Université de Montpellier, CNRS, IRD, EPHE, F-34095 Montpellier, France*

[c] *Departamento de Paleontología, Museo Nacional de Historia Natural, Calle 26 s/n, Cota Cota, La Paz, Estado Plurinacional de Bolivia*

[d] *Géosciences Montpellier, Université de Montpellier, CNRS, F-34095 Montpellier, France*

[*] Corresponding author e-mail address : mfernandezmonescillo@gmail.com (M. Fernández-Monescillo)

Abstract

We report here the first case of bilateral mandibular hypodontia for a notoungulate, further associated with exostosis on various limb bones. We describe a partial skeleton of a palaeopathological individual of the notoungulate mesotheriid *Plesiotypotherium achirense*, from the Upper Miocene site of Achiri, Bolivian Altiplano. The main

pathology is hypodontia of two first molars on both sides of the jaw. Other craniomandibular affliction, likely related to the latter pathology, are a striking overgrowth of two first upper molars on both sides and the anomalous development of masticatory muscle insertions (m. masseter, pterygoideus medialis, temporalis, and temporalis pars profundis). The pathological sequence of the masticatory apparatus was reconstructed in this individual according to distinctive wear of ever-growing crowns of two first upper molars, and the unequal lower alveoli reabsorption. Additional pathologies are exostoses observed on several articular surfaces of limb bones, from the scapula to distal phalanges. They likely decreased the range of movements during locomotion of this individual. Given its multiple pathologies, we might have expected this abnormal individual to be a potential easy prey. However, the long-time survival of this animal suggests a low predatory pressure in this area at that time, a hypothesis which is consistent with the virtual absence of flesh-eating vertebrates in the Achiri fossil record.

Key words: South America, late Neogene, Typotheria, *Plesiotypotherium*, palaeopathology, hypodontia, exostosis.

1. Introduction

Notoungulata are among the most successful and diversified South American mammalian clades in the Cenozoic, with a late Palaeocene–Holocene range (e.g., Simpson, 1948; McKenna and Bell 1997; Croft, 1999). Within species-rich rodent-like notoungulates (Typotheria; Reguero and Prevosti, 2010), Mesotheriidae include Trachytheriinae (Oligocene; Billet et al., 2008) and Mesotheriinae (Miocene–Pleistocene; Paz et al., 2011). In the Bolivian Altiplano, the Upper Miocene locality of Achiri (Pacajes Province, La Paz Department) was first reported by Hoffstetter et al. (1972). The most common taxon in Achiri is the mesotheriine *Plesiotypotherium*

achirense, with ca. 64% of the mammalian fossil specimens recovered (45 out of 70) (Fernández García, 2018). The excavations carried out in the Achiri area during the last decade have allowed for recovering cranial, mandibular, and postcranial remains of *P. achirense*, including a partial skeleton of a striking individual displaying multiple dental and skeletal pathologies (MNHN-Bol-V 12617). These palaeopathologies are mainly observed in the masticatory apparatus and in the postcranial skeleton. Pathologies were so far virtually undocumented among Notoungulata, with the noticeable exceptions of a few dental defects (enamel hypoplasia; *Toxodon* sp.; Braun et al., 2014), and postcranial exostoses (*Toxodon platensis*; Guérin and Faure, 2013) in Pleistocene toxodontids. To our knowledge, the individual MNHN-Bol-V 12617 is the first case of multiple osteo-dental pathologies formally described among Mesotheriidae. Noticeably, an individual of the late Oligocene mesotheriid *Trachytherus alloxus* with multiple broken limb bones subsequently healed has been recently reported (Croft, 2016), but it has not been described yet. In this paper we (1) describe the pathologies of this individual of *P. achirense* with respect to numerous asymptomatic specimens from the same taxon and locality, and (2) provide hypothetical palaeobiological inferences based on the long-lasting survival of this abnormal mesotheriine individual, and the scarce flesh-eating taxa evidence at Achiri at this time.

2. Material and methods

2.2. Material

2.2.1. Institutional abbreviations

MNHN-Bol, Museo Nacional de Historia Natural, La Paz, Bolivia; MNHN, Muséum national d'Histoire naturelle, Paris, France.

2.2.2. *Plesiotypotherium achirense* specimens

The pathological specimen MNHN-Bol-V 12617 of *Plesiotypotherium achirense* was unearthed at the top of the Cerro Pisakeri (Fig. 1A–B). All asymptomatic specimens used for comparison come from the same geological unit (Mauri Formation [Fm.], Unit IV), also in the Achiri area (Fig. 1B).

2.2.3. Systematic palaeontology

Order Notoungulata Roth 1903

Suborden Typotheria Zittel 1893

Family Mesotheriidae Alston 1876

Subfamily Mesotheriinae Alston 1876

Genus Plesiotypotherium Villarroel 1974

Plesiotypotherium achirense Villarroel 1974

(Figs. 2–5)

2.2.4. Measurements

We have used a digital calliper of 150 mm (precision ±0.1 mm). Measurement abbreviations (craniomandibular, dental, and postcranial) and the summary of the measurements of the study specimen and other *P. achirense* specimens appears in Supplementary Material 1.

2.2.5. X-ray tomography and 3D surface rendering

The skull and mandible of the pathological individual of *P. achirense* (MNHN-Bol-V 12617) and other asymptomatic cranial specimen (MNHN-Bol-V 8507) and mandible (MNHN-Bol-V 12669) were scanned in the MEDICENTRO clinic of La Paz, Bolivia, using a Phillips MX 8000 clinical CT Scanner (140Kv and 300 mA; 0.26 mm pixel size and 0.75 mm interslice). The digital surfaces (skull and mandible) were extracted using AVIZO 10.0 (FEI Visualization Sciences Group). The skull and mandible were generated by thresholding tool, while the dental reconstruction was made

manually slice by slice. Finally, the 3D surfaces were generated using unconstrained smoothing option with a value of ca. 3.5–4.

2.2.6. Anatomical description

The osteological terms follow the terminology of the Nomina Anatomica Veterinaria (Wible et al., 2005). As for orientation, we used the terms: anterior, posterior (occipital), dorsal, medial, and lateral (skull and mandible); mesial, distal, lingual, and labial (in teeth); medial (sagittal plane), lateral, cranial (dorsal in the manus and pes), caudal (palmar in the manus and plantar in the pes), proximal, and distal (appendicular skeleton). The pelvis and Mt I had not been previously reported for this taxon.

2.2.7. Dating

The fossil-yielding sedimentary series at Cerro Pisakeri includes five volcanic tuffs. We dated two tuffs immediately bracketing the pathological specimen: sample ACH-TUF3 and sample ACH-TUF4, which are located five metres beneath and ten metres above the MNHN-Bol-V 12617 specimen, respectively. We performed step-heating $^{40}Ar/^{39}Ar$ experiments on feldspar micro-populations (detailed methodology in online Supplementary Material 2). For the sample ACH-TUF3, we obtained a plateau age of 10.35 ± 0.07 Ma, corresponding to 57.4% of ^{39}Ar released (five steps; Supplementary Material 3). We also calculated for all steps an inverse isochron age of 10.42 ± 0.09 Ma with a MSWD = 4.55 and an initial $^{40}Ar/^{36}Ar$ ratio of 299.9 ± 2.3 (Supplementary Material 4), indicating that the trapped $^{40}Ar/^{36}Ar$ is indistinguishable from the atmospheric $^{40}Ar/^{36}Ar$. We retained the inverse isochron age at 10.42 ± 0.09 Ma for the tuff below the MNHN-Bol-V 12617 specimen. For the sample ACH-TUF4, we obtained a plateau age of 9.42 ± 0.1 Ma corresponding to 99.39% of ^{39}Ar released (Supplementary Material 5). These $^{40}Ar/^{39}Ar$ datings confirm that the fossil assemblage from the Cerro Pisakeri, including the pathological specimen, is Upper Miocene in age

126 (late Mayoan–early Chasicoan South American Land Mammal ages [SALMA], based
127 on Gradstein et al., 2012).
128
129 ***2.3. Description of the pathologies***
130 **2.3.1. Pathological descriptions**
131 We use the term hypodontia considered as the absence of teeth (less than six
132 teeth expect the third molars, primary or definitive dentition; Pemberton et al. 2005),
133 and related absent of teeth development (Al-Ani et al. 2017). The taxon *P. achirense*, as
134 member of the Mesotheriinae subfamily is characterized by hypselodontia (ever-
135 growing teeth; Gomes Rodrigues et al. 2017), therefore the teeth development is
136 increased during the life of the animal.
137 The term exostosis is used to refer to any outgrowth of a bone (bony spur) from
138 the cortical surface and is a more general term than the entity of osteochondroma, or
139 osseocartilaginous exostosis (Khurana 2008).
140 **2.3.2. Skull and upper teeth**
141 The skull of the pathological individual (MNHN-Bol-V 12617) does not show
142 any particular osteological deformation in its dorsal, anterior and occipital aspects (Fig.
143 1 Supplementary Material 1 A–D, Fig. 2A–D). In lateral views (Fig.1 Supplementary
144 Material 1 C–D), overgrown M1s and M2s stand out on both sides. The M1-M2s are not
145 pathological teeth *per se* (no unusual outline or cusp Bauplan), but unworn hypselodont
146 teeth instead, characterised by a striking overgrowth due to the absence of occlusion
147 with their missing lower counterparts (hypodonty of both m1 and m2; Fig.1
148 Supplementary Material 1 C–D, Fig. 2A–D). The CT-Scan M1-M2 reconstruction
149 discard any post-dead teeth ejection from the alveolus (Fig. 2 A-D). The M1s further
150 present an anomalous wear, with oblique mesial wear at the mesial border or protoloph

(not at the same occlusal plane than the crista 2-crochet or metaloph; Fig. 2A–D). The M2s show also an oblique wear at the distal border, affecting the metaloph and crista 2-crochet (not as the same plane than the protoloph; Fig. 2A–D). The M3s have developed a generic wear (Fig. 2A–D) with respect to specimens from other individuals (i.e. MNHN-Bol-V 8507; Fig. 2E–H).

2.3.3. Mandible and lower teeth

The mandible is the main pathological element of MNHN-Bol-V 12617 (Fig. 2 Supplementary Material 1 A–E) with respect to normal individuals (i.e. MNHN-Bol-V 12669, Fig. 2 Supplementary Material 1 F–G). The identified pathologies are: (1) a bilateral hypodontia of m1-m2 (Fig. 3A–D); (2) anomalous bone structures in the ventrolateral and ventromedial border of the right mandibular ramus (Fig. 2 Supplementary Material 1 A, C); (3) a rostrocaudal elongation of the left coronoid process (Fig. 2 Supplementary Material 1 B); and (4) an anomalous and rounded overgrowth of the enamel of the right i1 (Fig. 2 Supplementary Material 1 D). The alveoli of left and right m1s are closed, whereas those of m2s are still open but shows initial alveolar bone resorption (Fig. 3 C-D). Compared with other referred specimens (Fig. 2 Supplementary Material 1 4F–G), we further noticed a dorsal alveolar bone resorption, which affects the ventrodorsal height of the right mandibular ramus (Fig. 2 A-D). The p4 shows an oblique (distoventral orientation) wear, finishing in a remarkable mesial tip (Fig. 3A–D), absent in other assigned specimens (Fig. 3E–H). The m3 shows a normal occlusal wear, except for a slight rostroventral orientation (Fig. 3A–B), lacking in other individuals (Fig. 3E–F).

2.3.4. Postcranial skeleton (Axial and appendicular)

MNHN-Bol-V 12617 is well represented by postcranial remains: axis, C3 vertebra, both scapulae, both radii, left ulna, left Mc IV, right Mc V, left scaphoid (Fig. 3

176 Supplementary Material 1), fused sacrum and pelvis, left Mt I-III, V, left navicular, left
177 cuboids and left ectocuneiform (Fig.4 Supplementary Material 1). On the right scapula,
178 the suprahamatus process (metacromion; see Fernández-Monescillo et al. 2018) shows
179 an ossified callus, which could correspond to a fracture subsequently healed (Fig. 4A).
180 Most postcranial remains available show slight exostosis in their articular surfaces: (1)
181 the coronoid process and glenoid cavity of the scapula; (2) the lateral and medial
182 borders of the caput radii (radius head) (Fig. 4B–C); (3) both lateral and medial sides of
183 the proximal articular surface of Mc IV, Mc V, Mt II, Mt III and Mt V (Fig. 4E); (4) the
184 coronoid process and anconeus process edges on the fragmentary left ulna (Fig. 4D); (5)
185 the articular borders of carpals (scaphoid) and tarsals (navicular, ectocuneiform, and
186 cuboids); and (6) also the surrounded external articular borders in the proximal
187 epiphysis of the first phalanges (not second or third phalanges) of manus and pes (Fig.
188 4F).
189

190 **3. Discussion**

191 ***3.1. Masticatory apparatus pathology***

192 In humans, hypodontia is congenital and it seems to have a genetic component.
193 Although the genetic origin of this anomaly remains unknown, polymorphism in 5'
194 flanking region of the PAX9 gene (Peres et al., 2005) and AXIN2 (Mostowska et al.,
195 2006) have been associated with non-syndromic hypodontia in humans (Pemberton et
196 al., 2005, Al Ani et al. 2017). Hypodontia is considered as the most common dental
197 anomaly in any human populations (e.g., Pemberton et al., 2005; Altug-Atac and
198 Erdem, 2007; Al-Abdallah, 2015). Hypodontia affects different teeth or dental regions,
199 and this affliction differs according to the ethnic groups of humans: second mandibular
200 premolars in North American children (Clayton, 1956), lateral maxillary incisors in

Saudi Arabian children (Al-Emran, 1990), second maxillary premolar in European children (Grahnén, 1956), or lateral maxillary incisors followed by premolars in Turkish population (Altug-Atac and Erdem, 2007). Lavelle and Moore (1973) indicated primarily molar region affliction for humans. In human populations, the hypodontia occurs more often bilaterally than unilaterally (Silverman and Ackerman, 1979; Polder et al., 2004) or with almost similar percentage affliction (Al-Abdallah, 2015), and furthermore it is more common in the mandible (Wisth et al., 1974). Contrastingly, hypodontia affects mostly premolars and molars in other mammals (e.g., Cuesta Ruíz-Colmenares et al., 2004; Dacre, 2006). This dental pathology has been documented in domestic mammals like cats (Mestrinho et al., 2018), dogs (Pavlica et al., 2001) and equids (Dixon et al., 1999; Ramzan, 2001; Dacre, 2006; Easley, 2006).

In wild animals, hypodontia has been deeply documented in: (1) artiodactyls such as bighorn sheep (Lyman, 2010), Spanish wild goats (Vigal and Machordom, 1985; Gómez-Olivencia et al., 2011), mountain goat (Cowan and McCrory, 1970), wild Japanese serow (Natsume et al., 2005); and (2) primates, notably in Cercopithecoidea (Lavelle and Moore, 1973) and especially in colobines (Jablonski, 1992). By contrast, hypodontia has so far remained poorly documented in extinct mammals, with the exception of hypodontia reported on P4 of a lophiodontid perissodactyl from the Eocene of Spain (Cuesta Ruíz-Colmenares et al., 2004).

Hypodontia or dental affliction negatively impacts the masticatory function and global masticatory apparatus, as it can disrupt dental occlusion and constrain chewing movements as a result (Dixon and Dacre, 2005; Brown et al., 2008; Ardila and Montoya, 2009; Ali et al. 2014). It is documented in MNHN-Bol-V 12617 through the osteological anomaly noticed on the mandibular ramus, affecting the concerned muscular insertion. Indeed, the anomalous bone structure located on the ventrolateral

and ventromedial borders of the mandible likely impacted the insertion of the m. masseter and pterygoideus medialis, respectively (Fernández García, 2018). The rostrocaudal elongation of the coronoid process would also have affected the insertion of the m. temporalis laterally, and of the m. temporalis pars profundis medially (Fernández García, 2018). Accordingly, an anomalous chewing cycle can be inferred for this mesotheriid specimen. Given these observations, it may be expected that hypodontia pathology would have affected more severely the masticatory apparatus of taxa with hypselodont (i.e., mesotheriines) than hypsodont or brachydont dentition, due to extreme overgrowth of non-opposed counterparts.

The dental formula of adult mesotheriines is 1023/2013 (Francis, 1965; Thenius, 1989). The M3s erupt faster than permanent upper premolars (Gomes Rodrigues et al., 2017). The presence of DP2, DP3 and DP4 is confirmed by several authors (e.g., Kraglievich, 1934; Francis, 1965; Gomes Rodrigues et al., 2017). In mesotheriids, distinct patterns of dental development are documented in hypsodont trachytheriines and hypselodont mesotheriines (Gomes Rodrigues et al., 2017). Several studies have been focussed to identified the specific genes involved into the tooth development (Al-Ani et al. 2017). Over 300 genes are expressed and involved in tooth morphogenesis (Kapadia et al. 2007; Küchler et al. 2013; Alves-Ferreira et al. 2014). In the case of hypselodont (ever-growing) teeth observed in mousses the continuous tooth renewal capacity relies on epithelial and mesenchymal stem cells (Renvois and Michon 2014). The term “crown-to-root transition” designated for hypselodont teeth, is fundamental to keep the balance between the suppling cells of the crown and that of the root to holding the tooth in place (Renvois and Michon 2014). In murine molars (hypselodont) is evidence loss of epithelial Notch and mesenchymal FGF (fibroblast growth factor) signal, helping in the continuous growth of the molar crown (Harada et al. 2002,

Yokohama-Tamaki et al. 2008).

MNHN-Bol-V 12617 exhibits a complete adult upper and lower dental formula (without deciduous teeth), except for the absence of m1-m2. This dental anomaly is identified as a bilateral hypodontia that occurred with already definitive molars erupted. The absence of osseous displacement or bridging callous presence of the mandibular ramus would discard an osseous fracture event. Also, agenesis (no teeth formation) of m1-m2 is discarded by effectively wear trilobed pattern of upper molars counterparts. In addition, the alveolus of m2 still open, the smooth aspects of the surface of the surrounded areas of m1 and m2 alveoli, and the absence of any osseous tissue swelling, and its bilateral and symmetrical aspects most likely discard infection as a potential cause for this pathology. Thus, would tentatively relate it with genetical factors provably affecting the hypselodont epithelial stem cells or the molecular regulation.

According to the distinctive wear pattern of the crowns of hypselodont M1-M2, his distinct occlusal level reached, and the unequal alveolar reabsorption of m1-m2, the pathology of the masticatory apparatus can be sequentially reconstructed as follows:

(1) Initially, the upper and lower teeth occlusion would be non-pathological, this is inferred according to the trilobed occlusal pattern of the upper molars (M1-M3), with no closed crown (Fig. 5A);

(2) Posteriorly, mandibular hypodontia likely appeared first for m1. This is suggested taking into account the major M1 overgrowth (crista 2-crochet and metaloph) in comparison to M2, and a closed alveolus of the m1 (right and left; Fig. 5B);

(3) Finally, hypodontia would have occurred for m2, a last step inferred from the major crown wear of the protoloph and medial crista 2-crochet on M2 (compared to M1), and the maintain of an open alveolus of the m2 (in early stages of alveolar reabsorption) (Fig. 5C).

According to the pathological stages of the occlusal dental surfaces, it can be inferred that P3, P4, and the protoloph of M1 were partially worn by p4, and that the crista 2-crochet and entoloph of M2-M3 were eroded by m3. This growing sequence is likely to offer key information for morphofunctional studies of the masticatory apparatus in mesotheriids. On MNHN-Bol-V 12617, there is no evidence of enamel hypoplasia that is usually recognised as a sign of starvation or feeding stresses in mammals (Mead, 1999). Therefore, a long-time starvation for this individual is not suggested, although the craniomandibular pathologies may have limited the food intake. Indeed, m1-m2 hypodontia (during life time) associated with the extreme M1-M2 overgrowth have involved constrained/abnormal chewing movements, as highlighted by the anomalous muscular insertions of some maxillomandibular muscles, which have probably affected a normal feeding supply.

3.2. Postcranial pathologies

In mammals, postcranial pathologies identified as exostoses are identified in:

(1) modern wild animals such as bovids (e.g., *Tragelaphus* sp., *Addax nasomaculatus*, *Bison bison*, *Oryx gazella*; Greer et al., 1977), cervids (e.g., *Odocoileus virginianus*, *Cervus* sp.; Greer et al., 1977) felids (e.g., *Panthera leo*; Greer et al., 1977), canids (*Canis lupus*; Greer et al., 1977), mustelids (e.g., *Gulo gulo*; Greer et al., 1977, or *Lutra lutra*; Prummel, 1987), ailurids (*Ailurus fulgens*; Lynch et al., 2002), and also ursids (*Ursus arctos*; Bartosiewicz, 2002);

(2) modern domesticated animals such as cats (Pool and Carrig, 1972), dogs (Dingwall et al., 1970; Silver et al., 2001), and horses (Bertoni et al., 2012);

(3) and extinct animals such as cave bears (Torres et al., 2005), machairodontine felid carnivorans (Salesa et al., 2014), and South-American endemic mammals like

300 ground sloths (McDonald, 1989; Pujos et al., 2016), glyptodonts (*Glyptodon* sp.;
301 Gillette and Ray, 1981), and notoungulates (*Toxodon platensis*; Guérin and Faure,
302 2013).

303 When severe, an exostosis on a bone articulation decreases the range of
304 movements and causes pain (Bertoni et al., 2012; Gavanier and Blum, 2017). The
305 pathological condition of exostosis observed on MNHN-Bol-V 12617 is categorised as
306 level 2 (i.e., "showing a minor irregular bulging of bone") according to the classification
307 of Stilton et al. (2016). Although slight, the numerous exostoses observed on the
308 articular surfaces of the available postcranial elements of MNHN-Bol-V 12617 indicate
309 that this pathological individual of *Plesiotypotherium achirense* may have presented
310 such symptoms.

311 ***3.3. Palaeoecological inferences***

312 The vertebrate fauna from the Mauri 6 Fm. is dominated by *Plesiotypotherium,*
313 considered as a "guide fossil" for upper Miocene deposits of the Bolivian Altiplano
314 (Marshall et al., 1983). In Achiri, *P. achirense* is the dominant species with a prevalence
315 of ca. 64%, among other notoungulates (Toxodontidae and Hegetotheriidae),
316 xenarthrans (sloths and cingulates), and rodents.

317 Palaeo-floras from Cerro Jakko Kota are closely located (ca. 18 km) and almost
318 coeval to the Cerro Pisakeri assemblage (ca. 10.66 ± 0.06 Ma; Gregory-Wodzicki,
319 2002). They indicate mean annual temperatures (MAT) of 21.5ºC, mean annual
320 precipitations of 550 ± 180 mm, and mean growing season precipitations of 580 ± 160
321 mm (Gregory-Wodzicki, 2002). Moreover, these palaeo-floras allow estimating a
322 palaeo-elevation of 1,160 ± 600 m, which is almost 2,800 m lower than the current
323 elevation (Gregory-Wodzicki, 2002), and consistent with estimates of 1,200 ± 1,000 m
324 (Garzione et al., 2008) and 1,400 ± 400 m (Lamb, 2016) determined from isotopic

palaeo-elevation proxies. The upper Miocene palaeo-floras of the northern Altiplano and from other locations in the Central Andes suggest that a large portion of this region was covered by subtropical-dry forests under a subtropical-dry climate at moderate elevations (Gregory-Wodzicki, 2002 and references therein). Such palaeo-ecological conditions may have favoured the large development of mesotheriine notoungulates in the northern Altiplano during Upper Miocene times, more specifically at ca. 10 Ma. These conditions drastically changed during the Pliocene, with a noticeable cooling (MAT 8–9ºC; Gregory-Wodzicki et al., 1998) associated with a substantial rise of that region, up to modern height at ca. 4,000 m above sea level (Garzione et al., 2008; Lamb, 2016). These drastic abiotic changes affected mammalian communities of the northern Altiplano as demonstrated by the major faunal turnover recorded around the Miocene–Pliocene transition: mesotheriines (primarily *Plesiotypotherium*) were dominant during the upper Miocene whereas ground sloths became dominant during the Pliocene (Marshall et al., 1983; Pujos et al., 2016).

The only flesh-eating taxon attested in the Achiri assemblage is the sparassodontan metatherian *Borhyaenidium altiplanicus*, documented by a single specimen (MNHN-Bol-V 011889=ACH-0243, holotype; Villarroel and Marshall, 1983). In addition, there is no record either for prey birds, snakes, or crocodylians at Achiri (Villarroel and Marshall, 1983). Moreover, no predation mark has been identified on the available bone sample (old and new collects). Predators are known to mainly hunt substandard individuals (Temple, 1987; Genovart et al., 2010), as would be the case for the *Plesiotypotherium achirense* individual (MNHN-Bol-V 12617). According to that, due to its numerous pathologies of the chewing-cycle abnormalities, mostly evidenced in mandibular muscles insertion and extreme M1-M2 overgrowth, the normal feeding intake would be affected. Also, the postcranial pathologies (exostoses) would suggest a

restricted appendicular movement, that would identify as preferential prey for predators. The inferred long-termed multiple pathologies would have increased the probability for this mesotheriine of being hunted. Strikingly, no predation evidence is visible in this individual, and no other precise cause can be evoked for its death. This, together with the almost inexistent presence of flesh-eating taxa at Achiri at this time would suggest a very low predation pressure, thus confirming other observations in pre-GABI Cenozoic stages of South America with respect to other continental regions (e.g., Holarctic or Australian regions; Croft, 2006; Croft et al., 2018; Prevosti and Forasiepi, 2018).

4. Conclusions

The palaeo-ecological conditions inferred at the late Mayoan-early Chasicoan SALMAs (10 Ma) at the Bolivian Altiplane clearly favoured the dominant faunas (*Plesiotypotherium*, Mesotheriinae), while dramatical climatic change at the Mio-Pliocene transition identified the major faunal turnover with the major prevalence of ground sloths during the Pliocene.

The surprising encounter of the study sample MNHN-Bol-V 12617 of *P. achirense*, characterized by numerous and long-termed multiple paleopathologies (craniomandibular, dental, and postcranial) would identify as potential prey with increased chances to be hunted. This, together with the almost inexistent presence of flesh-eating taxa at Achiri at this time would suggest and confirming other observations in other Cenozoic stages of South America compared with other Australian or Holarctic regions.

Acknowledgments: We thank all the team members (M. A. Abello, S. Adnet, G. Billet, and M. B. Prámparo) who participated to the 2010-2015 field campaigns in Achiri. We

thank the staff of the MEDICENTRO clinic in La Paz (Bolivia) for providing access to CT Scan facilities. We warmly thank to Juan Esteban Rodriguez (http://juanestebanartwork.com/) because his exceptional reconstruction of *Plesiotypotherium achirense*. We are indebted to the people and local authorities from Achiri for facilitating our fieldwork during the 2010–2018 campaigns. We thank A. Iemmolo for his technical support during $^{40}Ar/^{39}Ar$ analyses. This project was made possible according to the cooperation agreement (Nº 864/2014) between the MNHN-Bol (Bolivia), the ISE-M (France), and the CONICET (Argentina). This work was financially supported by the ECOS-FonCyT program (A14U01), the National Geographic Society (NGS 9971–16), and by the "Investissements d'Avenir" grant managed by the "Agence Nationale de la Recherche" (CEBA, ANR–10–LABX–0025–01).

References

Al-Abdallah, M., 2015. Prevalence and Gender Distribution of Permanent Tooth Agenesis among Jordanian Dental Patients: A Cross-Sectional Survey. Jordan Medical Journal 49:241–251.

Al-Ani, A.H., Antoun, J.S., Thomson, W,T., Merriman, T,R; Farella, M., 2017. Hypodontia: An Update on Its Etiology, Classification, and Clinical Management. BioMed Research International. 9378325, 1-9.

Al-Emran, S., 1990. Prevalence of hypodontia and developmental malformation of permanent teeth in Saudi Arabian schoolchildren. British Journal of Orthodontics 17:115–118.

Ali, S.A., Hussain M., Naqvi, K., Khan, M.M., 2014. Myofacial Pain Dysfunction Syndrome (MPDS). Journal of the Pakistan Dental Association 23: 15-18.

400 Alston, E.R., 1876. On the classification of the Order Glires. Proceedings of The
401 Zoological Society 44:61–98.
402 Altug-Atac, A.T., D. Erdem., 2007. Prevalence and distribution of dental anomalies in
403 orthodontic patients. American Journal of Orthodontics and Dentofacial
404 Orthopedics 131:510–514.
405 Alves-Ferreira, M; Pinho, T., Sousa, A; Sequeiros, J; Lemos, C., Alonso, I., 2014.
406 Indentification of genetic risk factors formaxillary lateral incisor agenesis.
407 Journal of Dental Research 93: 452-458.
408 Ardila, C.M., L. Montoya., 2009. Desórdenes bucales equinos. Revista de Salud Animal
409 31:143–151.
410 Bartosiewicz, L. 2002., Pathological Lesions on Prehistoric Animal Remains from
411 Soutwest Asia; pp. 320–360 in H. Buitenhuis, M. Mashkour, A. M. Choyke, and
412 A H. Al-shyyab (eds.), Archaeozoology of the Near East V. ARC Publicatioes,
413 Groningen.
414 Bertoni, L., Forresu, D., Coudry, V., F. Audigie, F., Denoix, J-M., 2012. Exostoses on
415 the palmar or plantar aspects of the diaphysis of the third metacarpal or
416 metatarsal bone in horses: 16 cases (2001-2010). Journal of the American
417 Veterinary Medical Association 240:740–747.
418 Billet, G., C. De Muizon., Mamani Quispe, B., 2008. Late Oligocene mesotheriids
419 (Mammalia, Notoungulata) from Salla and Lacayani (Bolivia): implications for
420 basal mesotheriid phylogeny and distribution. Zoological Journal of the Linnean
421 Society 152:153-200.
422 Braun, P.R., Ribeiro, A.M., Ferigolo, J., 2014. Microstructural defects and enamel
423 hypoplasia in teeth of *Toxodon* Owen 1837 from the Pleistocene of Southern
424 Brazil, Lethaia 47:418-431.

425 Brown, S.L., Arkins, S., D. J. Shaw., Dixon, P.M., 2008. Occlusal angles of cheek teeth
426 in normal horses with dental disease. The Veterinary Record 162:807–808.
427 Clayton, J.M., 1956. Congenital dental anomalies occurring in 3557 children", ASDC
428 Journal of Dentristy for Children 23:206–208.
429 Cowan, I.M., McCrory, W., 1970. Variation in the Mountain Goat, *Oreamnos*
430 *americanus* (Blainville). Journal of Mammalogy 51:60–73.
431 pp.
432 Croft, D. A., 1999. Placentals: endemic American ungulates; pp. 890–906 in R. Singer
433 (ed), Encyclopedia of Paleontology. Fitzroy Dearborn Publishers. Chicago.
434 Croft, D. A., 2006. Do marsupials make good predators? Insight from predato-prey
435 diversity ratios. Evolutionary Research 8: 1193–1214.
436 Croft, D. A., 2016. Horned Armadillos and Rafting Monkeys. The Fascinating Fossil
437 Mammals of South America (Life of The Past). Indiana University Press. 320.
438 Croft, D. A., Engelman, R.K., Dolgushina, T., Wesney, G., 2018. Diversity and disparity
439 of sparassodonts (Metatheria) reveal non-analogue nature of ancient South
440 American mammalian carnivore guilds. Proceedins B of the Linnean Society.
441 285:20172012.
442 Cuesta Ruíz-Colmenares, M.A., Jiménez Fuentes, E., Pérez Pérez, P. J., 2004. Un caso
443 de Hipodoncia en un lofiodóntido (Perissodactyla, Mammalia) del Eoceno
444 Medio de la Cuenca del Duero (Castilla y León, España). Interpretación a luz de
445 la agenesia dentaria humana. Revista Española de Paleontología 19:145–150.
446 Dacre, K., 2006. Applied Equine Dental Development. American Association of Equine
447 Practitioners, Indianapolis.
448 Dingwall, J.S., Pass, D.A., Pennock, P.W., Cawley, A.J., 1970. Case report. Multiple
449 cartilaginous exostoses in a dog. The Canadian Veterinary Journal 11:114–119.

450 Dixon, P.M., Dacre, I., 2005. A review of equine dental disorders. Veterinary Journal
451 169:165–187.
452 Dixon, P.M., Tremaine, W.H., Pickles, K., Kuhns, L., Hawe, C., Maccan, J., McGorum,
453 B.C., Railton, D.R., Brammer, S., 1999. Equine dental disease part 2: a long-
454 term study of 400 cases: disorders of development and eruption and variations in
455 position of the cheek teeth. Equine Veterinary Journal 31:519–528.
456 Easley, J. 2006. Equine Dental Developmental Abnormalities. American Association of
457 Equine Practitioners. Indianapolis.
458 Fernández García, M. 2018. Descripción dentaria y osteológica, anatomía funcional,
459 paleoneurología, sistemática y filogenia de la familia Mesotheriidae (Mammalia,
460 Notoungulata). PhD dissertation, Universidad Nacional de Cuyo, Mendoza,
461 Argentina, 385 pp.
462 Fernández-Monescillo, M., Mamani Quispe, B., François, P., Antoine, P-O., 2018.
463 Functional Anatomy of the Forelimb of *Plesiotypotherium achirense*
464 (Mammalia, Notoungulata, Mesotheriidae) and Evolutionary Insights at the
465 Family level. Journal of Mammalian Evolution. 25: 197-211.
466 Francis, J. C. 1965. Los géneros de la subfamilia mesotheriinae (Typotheria,
467 Notoungulata) de la República Argentina. Boletín del Laboratorio de
468 Paleontología de Vertebrados 1:7–31.
469 Garzione, C.N., Hoke, G.D., Libarkin, J.C., Withers, S., Macfadden, B., Eiler, J., Ghosh,
470 J.P, Mulch, A., 2008. Rise of the Andes. Science 320:1304–1307.
471 Gavanier, M., A. Blum, A., 2017. Imaging of benign complications of exostoses of the
472 shoulder, pelvic girdles and appendicular skeleton. Diagnostic and Interventional
473 Imaging 98:21–28.

474 Genovart, M., Negre, N., Tavecchia, G., Bistuer, A., Parpal, L., Oro, D. 2010., The
475 Young, the Weak and the Sick: Evidence of Natural Selection by Predation.
476 PLoS One 5:e9774.
477 Gillette, D.D., Ray, C.E., 1981. Glyptodonts of North America. Smithsonian
478 Contitributions Paleobiology 255.
479 Gomes Rodrigues, H., Herrel, A., G. Billet, G., 2017. Ontogenetic and life history trait
480 changes associated with convergent ecological specializations in extinct
481 ungulate mammals. Proceedings of the National Academy of Sciences of the
482 United States of America 114:1069–1074.
483 Gómez-Olivencia, A., Arcederedillo, D., Rios-Garaizar, J., Garate, D., Iriarte, E.,
484 Ziortza San Pedro., 2011. Dental Anomalies in the Mandible of *Capra*
485 *pirenaica*: Presence of Two Permanent fourth Premolars in a Pleistocene Wild
486 Goat from Arlanpe Cave (Bizkaia, Northern Spain). International Journal of
487 Osteoarchaeology 23:737–745.
488 Gradstein, F.M., Ogg, J.G., Schmitz, M.D., Ogg, G.M., 2012. The Geological Time
489 Scale 2012. Volume 2. Amsterdam, Elsevier.
490 Grahnén, H., 1956. Hypodontia in the permanent dentition. A clinical and genetical
491 investigation. Odontologisk Revy 7:5–100.
492 Greer, M., Greer,J.K., Gilligham, J., 1977. Osteoarthritis in Selected Wild Mammals.
493 Proceedings of the Oklahoma Academy of Science 57:39–43.
494 Gregory-Wodzicki, K.M., Mcintosh, W.C., Velasquez, K., 1998. Climatic and tectonic
495 implications of the late Miocene Jakokkota flora, Bolivian Altiplano. Journal of
496 South American Earth Sciences 11:533–560.
497 Gregory-Wodzicki, K. M., 2002. A late Miocene subtropical-dry flora from the northern
498 Altiplano, Bolivia. Palaeogeography, Palaeoclimatology, Palaeoecology

499 180:331–348.
500 Guérin, C., Faure, M., 2013. Un Nouveau Toxodontidae (Mammalia, Notoungulata) du
501 Pléistocène supérieur du Nordeste du Brésil. Geodiversitas 36:155–205.
502 Hoffstetter, R; C. Martinez; M., and P. Tomasi. 1972. Nouveaux gisement de
503 Mammifères néogènes dans les couches rouges de l´Altiplano bolivien. Comptes
504 Rendus de l'Académie des Sciences Paris 275:739-742.
505 Jablonski, N.G., 1992. Dental agenesis as evidence of possible genetic isolation on the
506 colobine monkey, *Rhinopithecus roxellana*. Primates 33:371–376.
507 Kapadia, H., Mues, G., D'Souza, R., 2007. Genes affection tooth morphogenesis.
508 Orthodontics and Craniofacial Research 93: 237-244.
509 Khurana, J.S. Bone Pathology. Humana Press. 416 pp.
510 Kraglievich, L., 1934. La antigüedad pliocena de las faunas de Monte Hermoso y
511 Chapadmalalal deducidas de su comparación con las que le precedieron y
512 sucedieron. Imprenta El Siglo ilustrado. Montevideo 939:1- 136.
513 Küchler, E.C., A. Lips, A., Tannure, P.N., Ho, B.; Costa, M.C., Granjeiro, J.M., Vieira,
514 A.R. Tooth agenesis association with self-reported family history of cancer.
515 Journal of Dental Research 92: 149-155.
516 Lamb, S. 2016., Cenozoic uplift of the Central Andes in northern Chile and Bolivia–
517 reconciling paleoaltimetry with the geological evolution. Canadian Journal of
518 Earth Sciences 53:1227–1245.
519 Lavelle, C.L., Moore, W.J., 1973. The Incidence of Agenesis and Polygenesis in the
520 Primate Dentition. American Journal of Physical Anthropology 38:671-679.
521 Lyman, R.L., 2010. Mandibular Hypodontia and Osteoarthritis in Prehistoric Bighorn
522 Sheep (*Ovis canadensis*) in Eastern Washington State. USA. International
523 Journal of Osteoarchaeology 20:396–404.

524 Lynch M., McCraken, H., Scolocombe, R., 2002. Hyperostotic bone disease in red
525 pandas (*Ailurus fulgens*). Journal of Zoo and Wildlife Medicine 33:263–271.
526 Marshall, L. G., Hoffstetter, R., Pascual, R., 1983. Mammals and Stratigraphy:
527 Geochronology of the Continental Mammal-Bearing Tertiary of South America.
528 Palaeovertebrata 1-93.
529 McDonald, H. G. 1989., Not all ground sloth bones are pathological: but some are.
530 Journal of Vertebrate Paleontology 9:32A.
531 McKenna, M., Bell, S.K., 1997. Classification of Mammals: Above the Species Level.
532 Columbia University Press, New York, 640 pp.
533 Mead, A.J., 1999. Enamel hypoplasia in Miocene rhinoceroses (*Teleoceras*) from
534 Nebraska: evidence of severe physiological stress. Journal of Vertebrate
535 Paleontology 19:391–397.
536 Mestrinho, L.A., Louro, J.M., Gordo, I.S., Niza, M.M.R.E., Requicha, J. F., Force, J.G.,
537 Gawor, P., 2018. Oral and dental anomalies in purebred, brachycephalic Persian
538 and Exotic cats. Journal of the American Veterinary Medical Association
539 253:66–72.
540 Mostowska, A., Briedzia, B., Jagodziniski, P.P., 2006. Axis inhibition protein (AXIN2)
541 polymorphisms may be a risk factor for selective tooth agenesis. Journal of
542 Human Genetic 51:262-266.
543 Natsume, A., Koyasu, K., Hanamura, H., Nakagaski, H., Oda, S., 2005. Variation in the
544 number of teeth in wild Japanese serow (*Naemorhedus crispus*). Archives of
545 Oral Biology 50:849–860.
546 Pavlica, Z., Erjavec, V., Petelin, M., 2001. Teeth abnormalities in the dog. Acta
547 Veterinaria Brno 70:65–72.
548 Paz, R., Kramarz, A., Bond, M., 2011. Mesotheriid (Mammalia, Notoungulata) remains

549 from the Colhuehuapian Beds (Early Miocene) of Chichinales Formation, Río
550 Negro Province, Argentina. Ameghiniana 48:264–269.
551 Pemberton, T.J., Das, P., Patel, P.I., 2005. Hypodontia: genetics and future perspectives.
552 Brazilian Journal of Oral Sciences 4:695–706.
553 Peres, R.C.R., Scarel-Caminaga, R.M., Santo, A.R.R., Line S.R.P., 2005. Association
554 between PAX-9 promoter polymorphisms and hypodontia in humans. Archives
555 of Oral Biology 50:861–871.
556 Polder M.A., Van't Hof, M.A., Van Der Linden, F.P., Kuijpers-Jagtman, A.M., 2004. A
557 meta-analysis of the prevalence of dental agenesis of permanent teeth.
558 Community Dentistry and Oral Epidemiology 32:217–226.
559 Pool, R.R., Carrig, C.B., 1972. Multiple Cartilaginous Exostoses in a Cat. Vertebrate
560 Pathology 9:350–359.
561 Prevosti, F.J., Forasiepi, A.M., 2018. Evolution of South American Mammalian
562 Predators During the Cenozoic: Paleobiogeographic and Paleoenvironmental
563 Contingencies. Springer Geology. 196 pp.
564 Prummel, W., 1987. The faunal remains from the Neolithic site of Hekelingen III.
565 Helinium 27:190–258.
566 Pujos, F., De Iuliis, G., Mamani Quispe, B., Adnet, S., Andrade Flores, R., Billet, G.,
567 Fernández-Monescillo, M., Marivaux, L., Münch, P., Prámparo, M.B., and
568 Antoine, P-O., 2016. A new nothrotheriid xenarthran from the early Pliocene of
569 Pomata-Ayte (Bolivia): new insights into the caniniform-molariform transition in
570 sloths. Zoologial Journal of the Linnean Society 178:679-712.
571 Ramzan, P.H., Dixont, P. M., Kempson, S.A., Rossdale, P.D., 2001. Dental dysplasia
572 and oligodontia in a throughbred colt. Equine Veterinary Journal 33:99–104.
573 Reguero. M.A., Prevosti, F.J., 2010. Rodent-like notoungulates (Typotheria) from Gran

574 Barranca, Chubut Province, Argentina: phylogeny and systematics; pp. 148–165
575 in Madden, R. H. Carlini, H. H., Vucetich, M. G, and Kay, R. F (eds). The
576 Paleontology of Gran Barranca: Evolution and Environmental Change through
577 the Middle Cenozoic of Patagonia. Cambridge University Press, Cambridge.
578 Roth, S., 1903. Los ungulados sudamericanos. Anales del Museo de La Plata. Sección
579 Paleontologia, 5:1–36.
580 Salesa M.J., Anton, M., Siliceo, G., Pesquero, M.D., Alcala, L., 2014. First evidence of
581 pathology in the forelimb of the late Miocene saber-toothed felid
582 *Promegantereon ogygia* (Machairodontinae, Smilodontini). Anatomical Record
583 297:1090–1095.
584 Silver, G.M., Bargley, R.S., Gavin, P.R., Kippenes, H., 2001. Radiographic diagnosis:
585 cartilaginous exostoses in a dog. Veterinary Radiology and Ultrasound 42:231–
586 234.
587 Silverman N.E., Ackerman, J.L., 1979. Oligodontia: a study of its prevalence and
588 variation in 4032 children. Journal of Dentistry for Children 46:470–477.
589 Simpson G.G., 1948. The beginning of the age of mammals in South America Part 1.
590 Systematics: Marsupialia, Edentata, Condylarthra, Litopterna and
591 Notioprogonia, Bulletin American Museum of Natural History 91:1–232.
592 Stilton K.T., Hopkins, S.S.B., Davis, E.B., 2016. Osteopathology in Rhinocerotidae
593 from 50 Million Years to the Present. PLoS One 11:e0146221.
594 Temple S.A., 1987. Do Predators Always Capture Substandard Individuals
595 Disproportionately From Prey Populations?. Ecology 68:669–674.
596 Thenius, E., 1989. Mammalia: Zähne ung Gebiss der Säugetiere in J. Niethammer, H.
597 Schliemann, and D. Starck (eds.) Handbuch der Zooologie, Volume 8. Verlag
598 Walter de Gruyter and Co. Berlin. 513 pp. [German 1–164].

599 Torres, T de., Ortiz, J.E., Cobo, R, Julià, R., Camacho, A., Puch, C., Llamas, J.F., 2005.
600 Presence of two cave bear species in La Lucia cave (Lamasón, Cantabria, N
601 Spain): *Ursus deningeri* von Reichenau and *Ursus spelaeus* Rosenmüller-
602 Heinroth. MUNIBE Antropologia-Arkeologia 57;103–122.
603 Vigal, C. R., Machordom, A., 1985. Tooth Eruption and Replacement in the Spanish
604 Wild Goat. Acta Theriologica 30:305–320.
605 Villarroel, C., 1974. Les mésothérinés (Notoungulata, Mammalia) du Pliocène de
606 Bolivie et leurs rapport avec ceux d'Argentine. Annales de Paléontologie
607 60:245–281. [French 245–281]
608 Villarroel, C., Marshall, L. G., 1983. Two New Late tertiary Marsupials
609 (Hathlyacyninae and Sparassocyninae) from the Bolivian Atiplano. Journal of
610 Paleontology 57:1061–1066.
611 Waibl, H., Gasse,H., Hashimoto, Y., 2005. Nomina Anatomica Veterinaria. Hannover:
612 International Committee on Veterinary Gross Anatomical Nomenclature, World
613 Association of Veterinary Anatomis, Hannover.
614 Wisth, P.J., Thunold, K., Böe, O.E., 1974. Frequency of hypodontia in relation to tooth
615 size and dental arch width. Acta Odontologica Scandinavica 32: 201-206.
616 Zittel, K.A., 1893. Handbuch der Palaeontologie, Volume IV. Vertebrata (Mammalia).
617 Druck und Verlag von R. Oldenbourg, Munchen und Leipzig, 590 pp.
618
619

620 **Figure Captions**

621 Figure 1. Location map of Achiri, Pacajes Province, La Paz Department, Bolivia.
622 General map of Bolivia (a), detailed map showing the location of the Mauri and Ulloma
623 formations, and hills ('cerros') surrounding the Achiri Village (b). [prepared for page
624 width]

625

626 Figure 2. Skulls of *Plesiotypotherium achirense* with digital reconstruction of the teeth.
627 Pathological skull (MNHN-Bol-V12617) (a-d), non-pathological skull (MNHN-Bol-V
628 8507) in mirror view (e-h). Lateral right views (a-b, e-f); ventral views (c-d, g-h). In
629 pink color and "º" the upper premolars (P3-P4), in red the upper molars (M1-M2), and
630 "*" appear the deformed overgrown M1-M2. In grey appears the usual aspect of upper
631 teeth of *Plesiotypotherium achirense.* Scale bar represents 5 cm. [prepared for page
632 width]

633

634 Figure 3. Mandible of *Plesiotypotherium achirense* with digital reconstruction of the
635 teeth. Pathological mandible (MNHN -Bol-V 12617) (a-d); mandible of
636 *Plesiotypotherium achirense* (MNHN-Bol-V 12669) (e-f). Right lateral views (a-b, e-f);
637 occlusal views (c-d, g-h). In red color and "*" are figured the pathological p4. In grey
638 appears the usual aspects of lower teeth. Scale bar represents 5 cm. [prepared for full
639 page width]

640

641 Figure 4**.** Skeletal reconstruction of the pathological individual of *Plesiotypotherium*
642 *achirense* from Achiri, with distinct osteological pathologies of postcranial elements
643 (MNHN-Bol-V 12617); blue denotes osteological remains that were unearthed. Lateral
644 view of the right scapula showing the osteological callus in the hamatus process

(acromion) (a); Head of the radius in cranial and proximal views respectively (b-c); Proximal epiphysis of the ulna in medial view (d); Mt III in proximal view (e); Second phalanx of the pes in dorsal view (f). Exostosis as visible in the articular edges (b-d); in addition, show a weak cortical bone structure in their broken areas (c-d). Reconstruction of *Plesiotypotherium achirense* made by Juan Esteban Rodriguez (http://juanestebanartwork.com/). [prepared for page width]

Figure 5. Pathological occlusal sequence reconstruction (upper left molar premolar series and lower left molar-premolar series) during the life time of *Plesiotypotherium achirense* (MNHN-Bol-V 12617). Early stages of occlusion (typical stage) (a); hypodontia of m1 and overgrowth of the crista 2-crochet and metaloph of the M1 (b); hypodontia of m2 and overgrowth of the mesial part (protoloph and parastyle) area of the M2 (c). Black dotted lines and "*" show the M1-M2 overgrown. [prepared for column width]

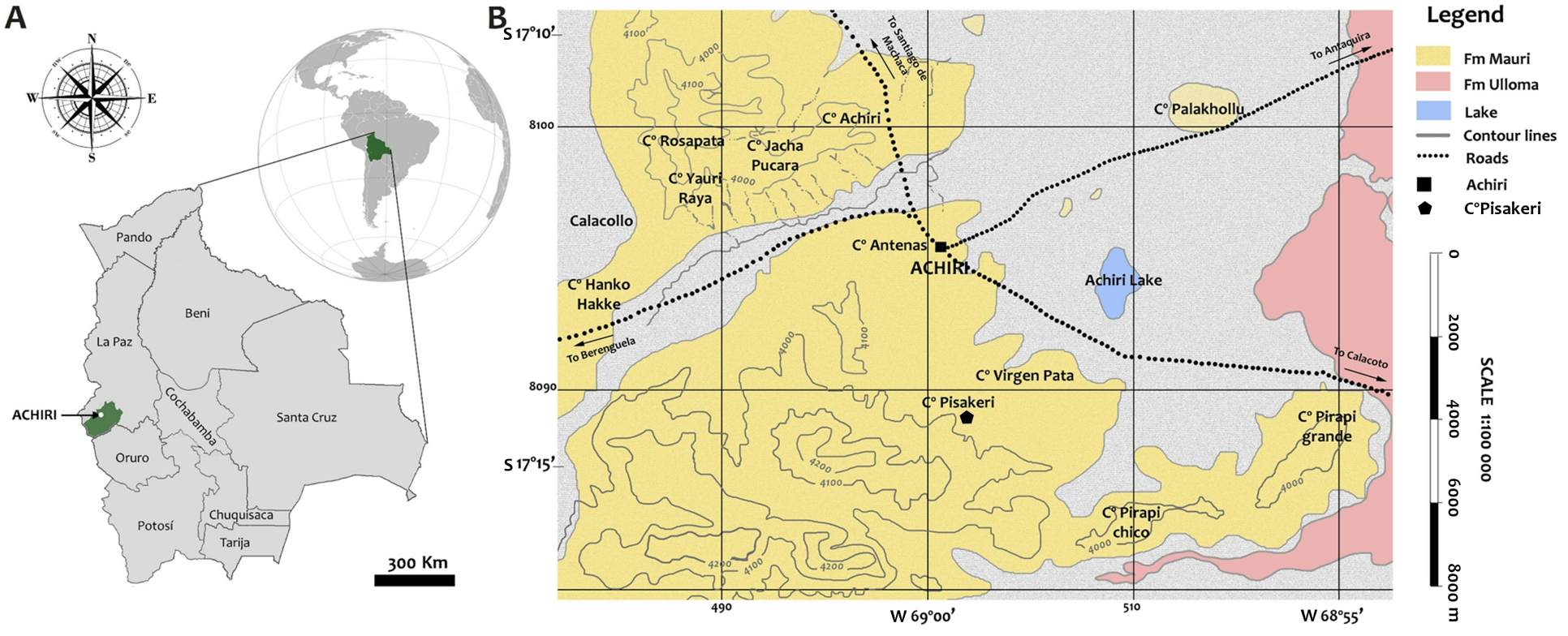
A
N
S
W
E
Pando
Beni
La Paz
Cochabamba
Santa Cruz
Oruro
Potosí
Chuquisaca
Tarija
ACHIRI
300 Km
B
S 17°10'
S 17°15'
8100
8090
490
510
W 69°00'
W 68°55'
To Santiago de Machaca
To Antaquira
To Berenguela
To Calacoto
C° Achiri
C° Palakhollu
C° Rosapata
C° Jacha Pucara
C° Yauri Raya
Calacollo
C° Antenas
ACHIRI
C° Hanko Hakke
Achiri Lake
C° Virgen Pata
C° Pisakeri
C° Pirapi grande
C° Pirapi chico
4100
4000
4200
Legend
Fm Mauri
Fm Ulloma
Lake
Contour lines
Roads
Achiri
C°Pisakeri
0
2000
4000
6000
8000 m
SCALE 1:100 000

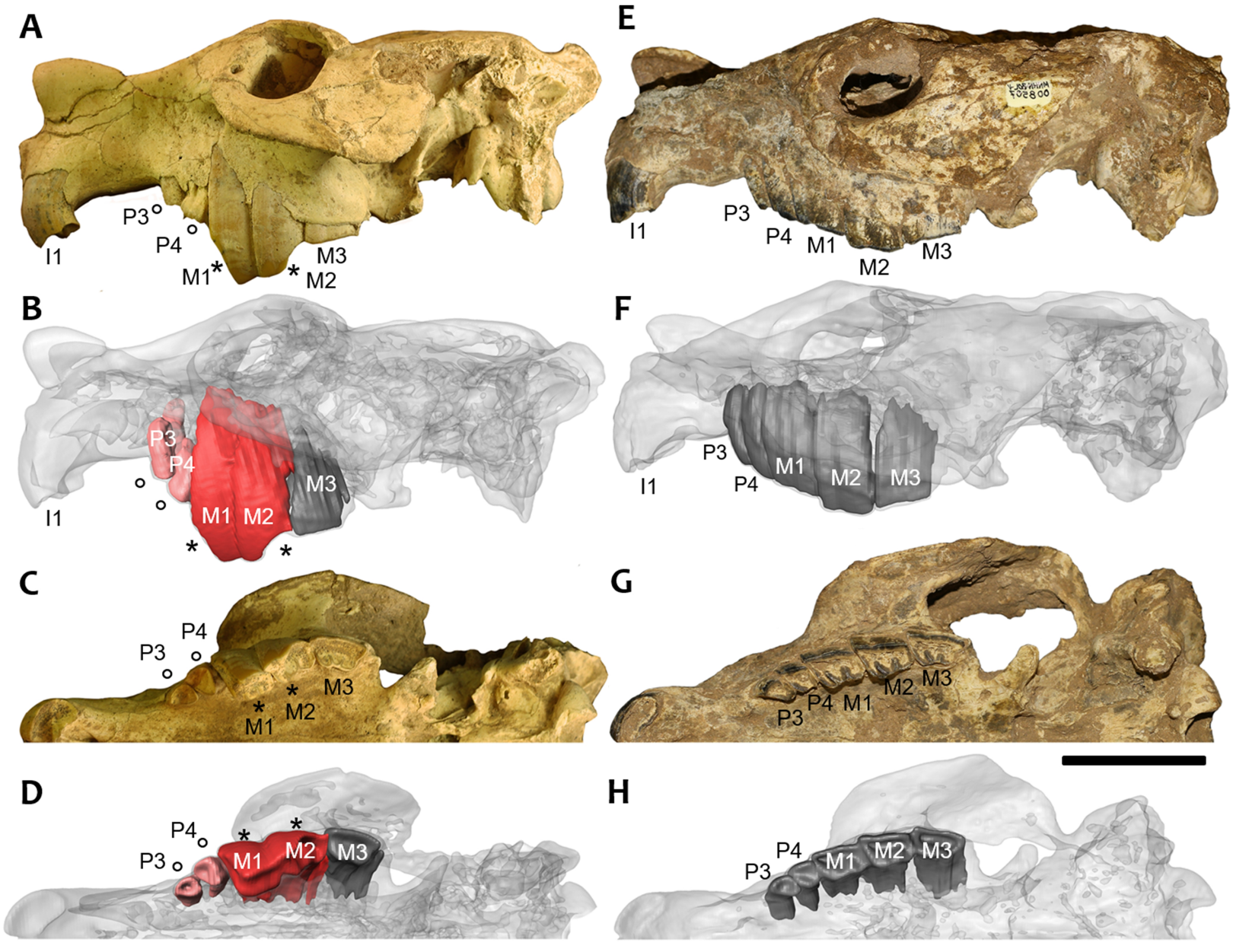
A
I1
P3
P4
M1
M2
M3
E
I1
P3
P4
M1
M2
M3
B
I1
P3
P4
M1
M2
M3
F
I1
P3
P4
M1
M2
M3
C
P3
P4
M1
M2
M3
G
P3
P4
M1
M2
M3
D
P3
P4
M1
M2
M3
H
P3
P4
M1
M2
M3

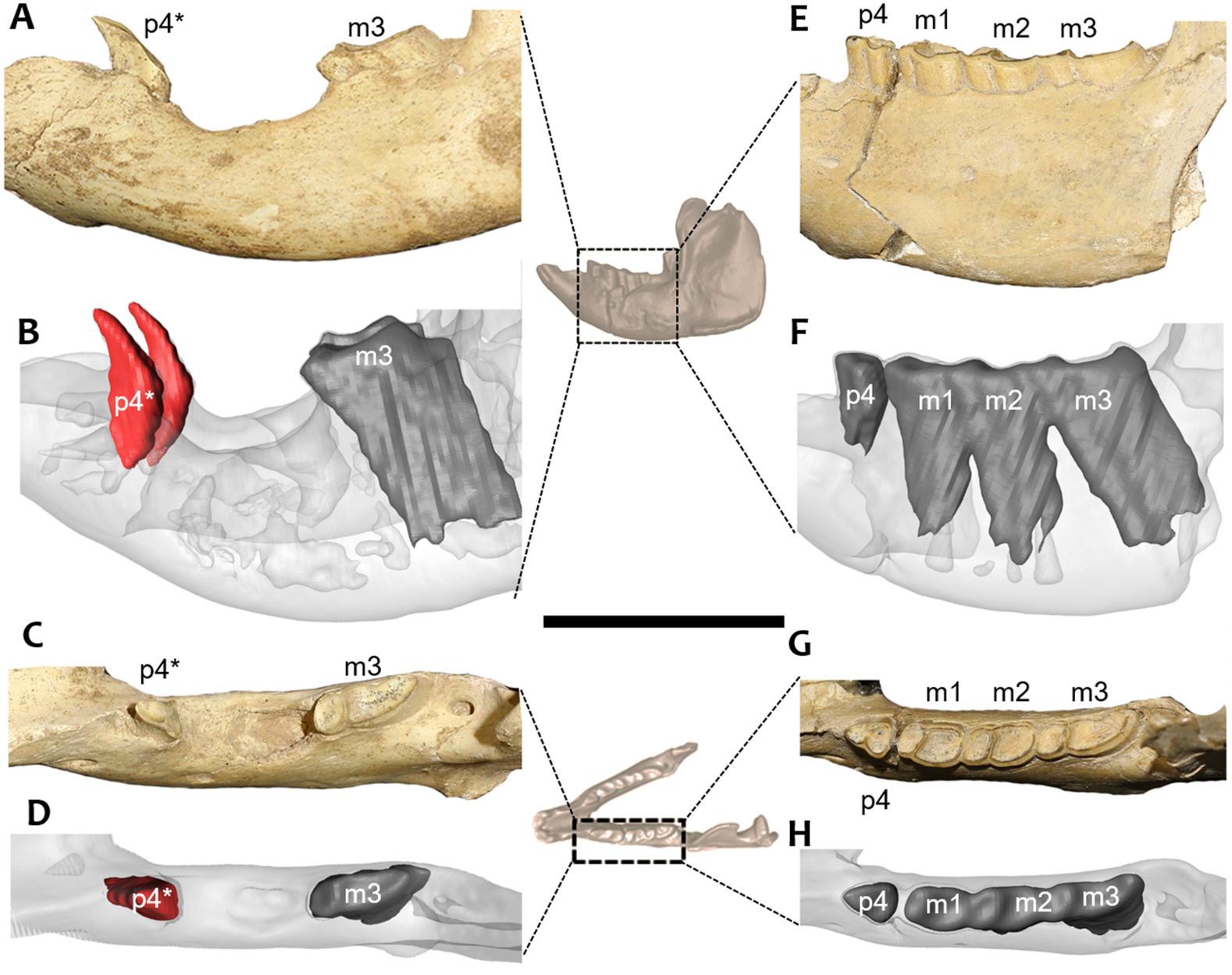
A
p4*
m3
B
p4*
m3
C
p4*
m3
D
p4*
m3
E
p4
m1
m2
m3
F
p4
m1
m2
m3
G
m1
m2
m3
p4
H
p4
m1
m2
m3

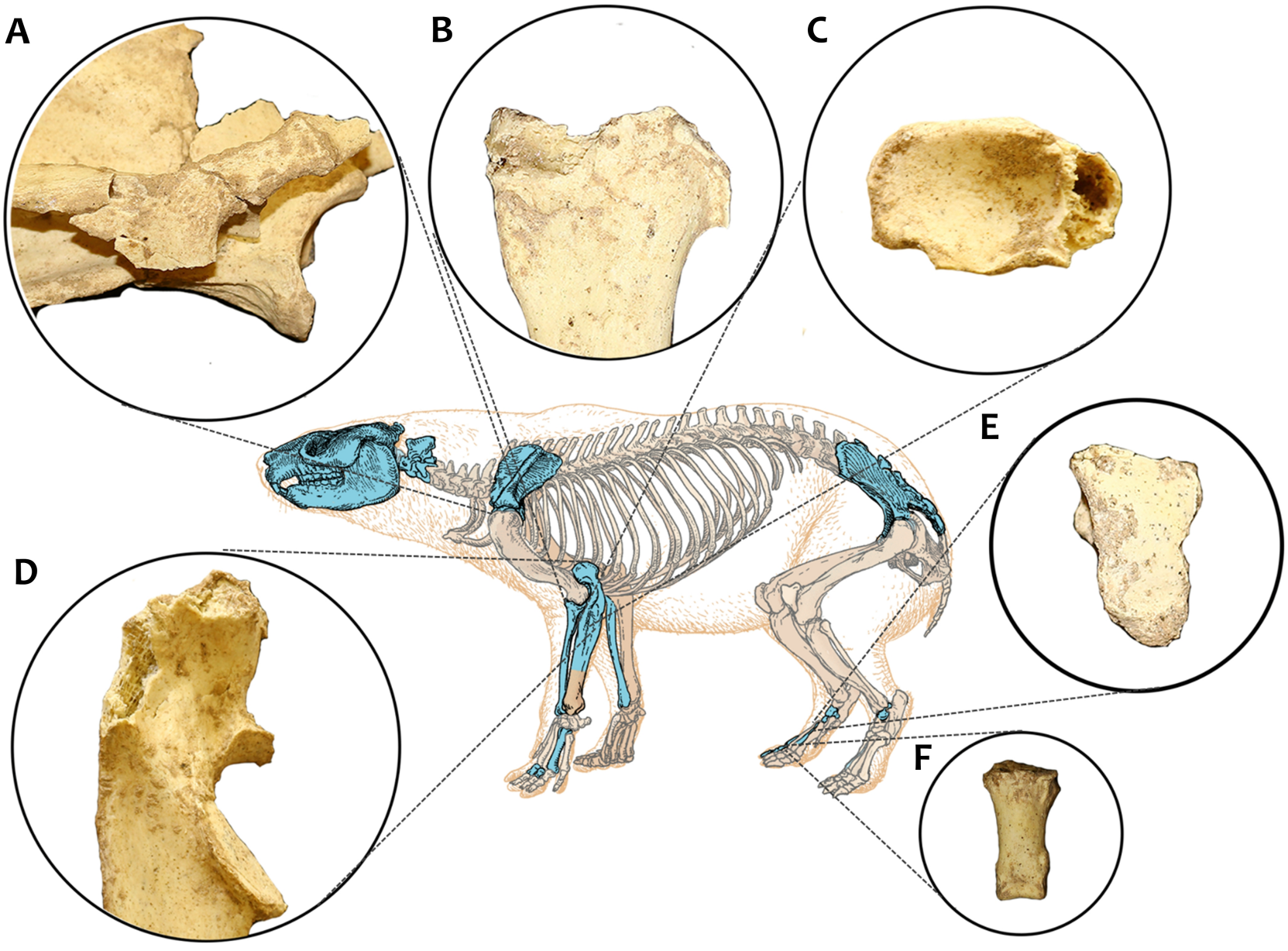
A
B
C
D
E
F

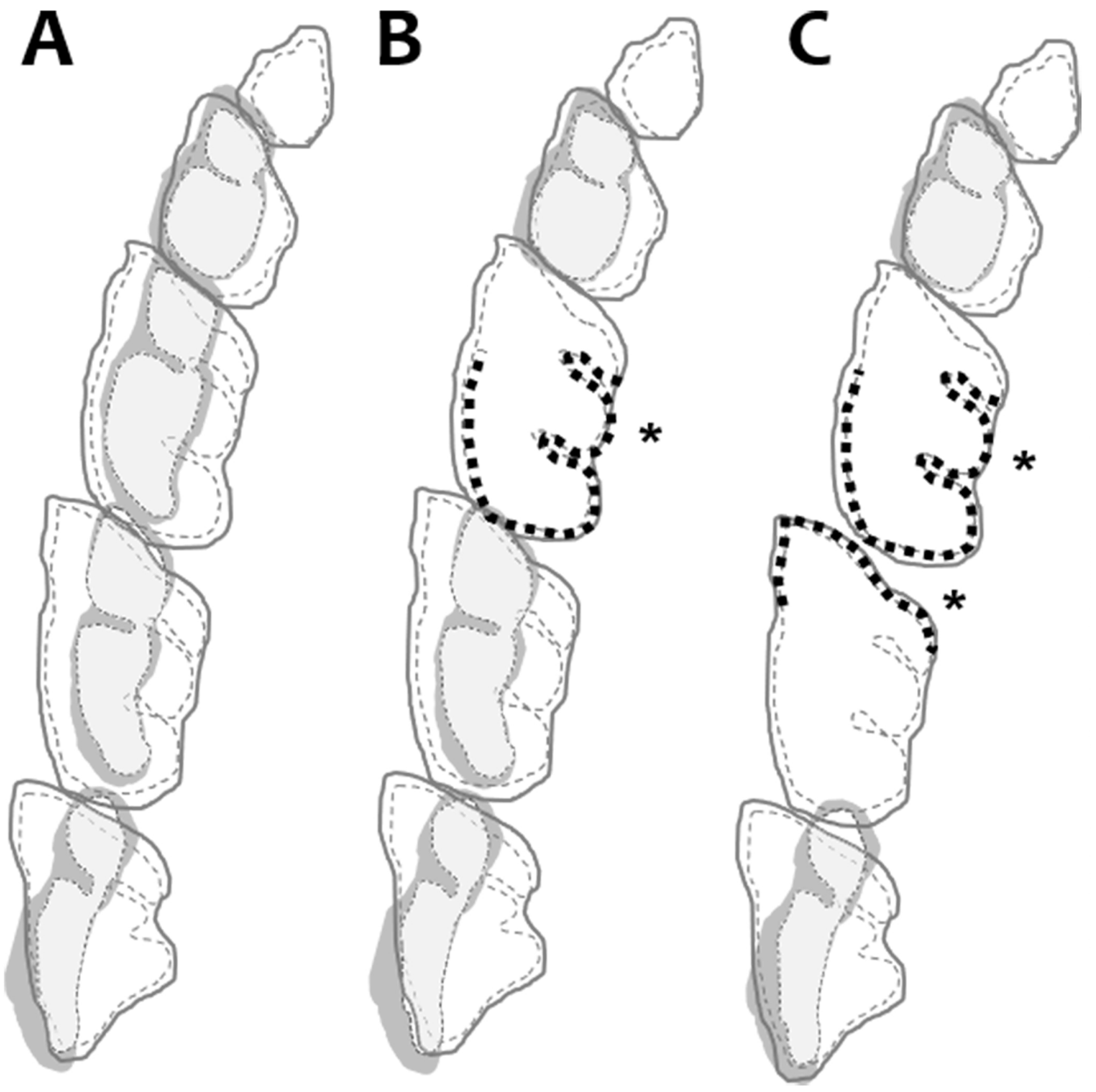
A
B
C
*
*
*

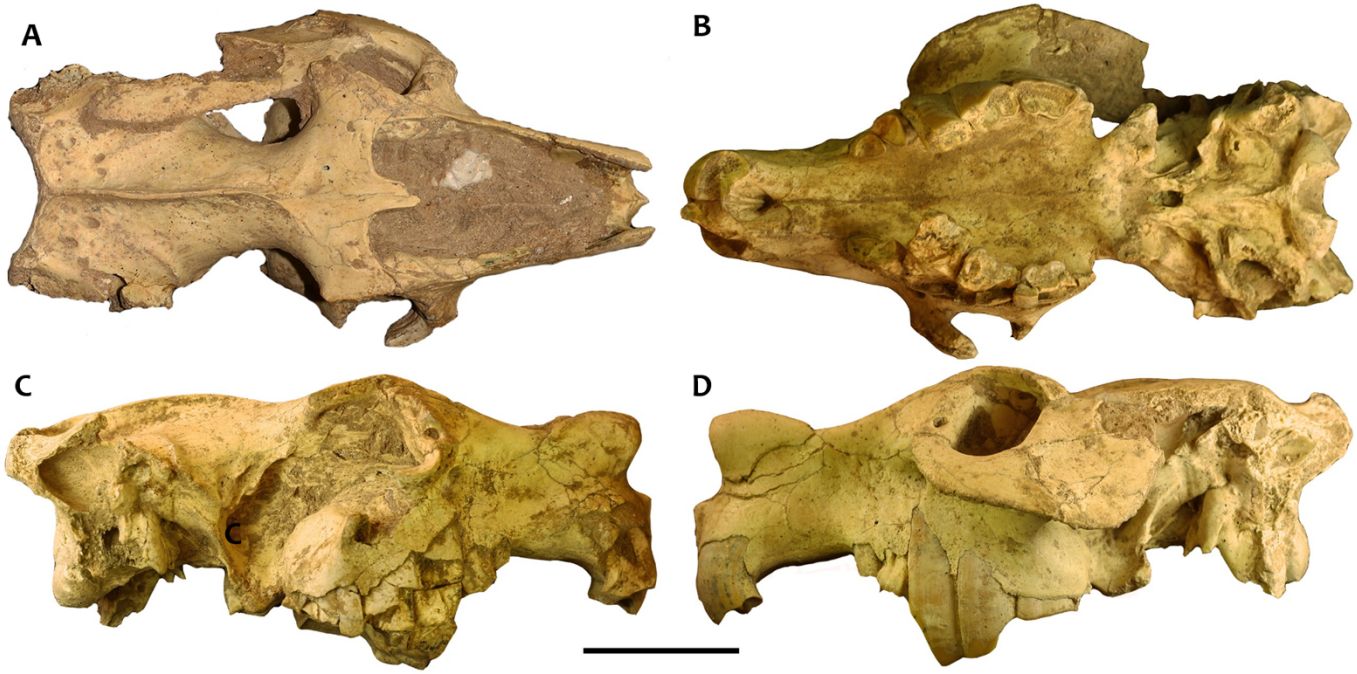

Figure 1 Supplementary material 1. Pathological skull of the mesotheriid notoungulate *Plesiotypotherium achirense* (MNHN-Bol-V 12617), from the late Miocene of Achiri, Bolivia. Dorsal (a); ventral (b); lateral right (c); lateral left (d) views. Scale bar represents 5 cm.

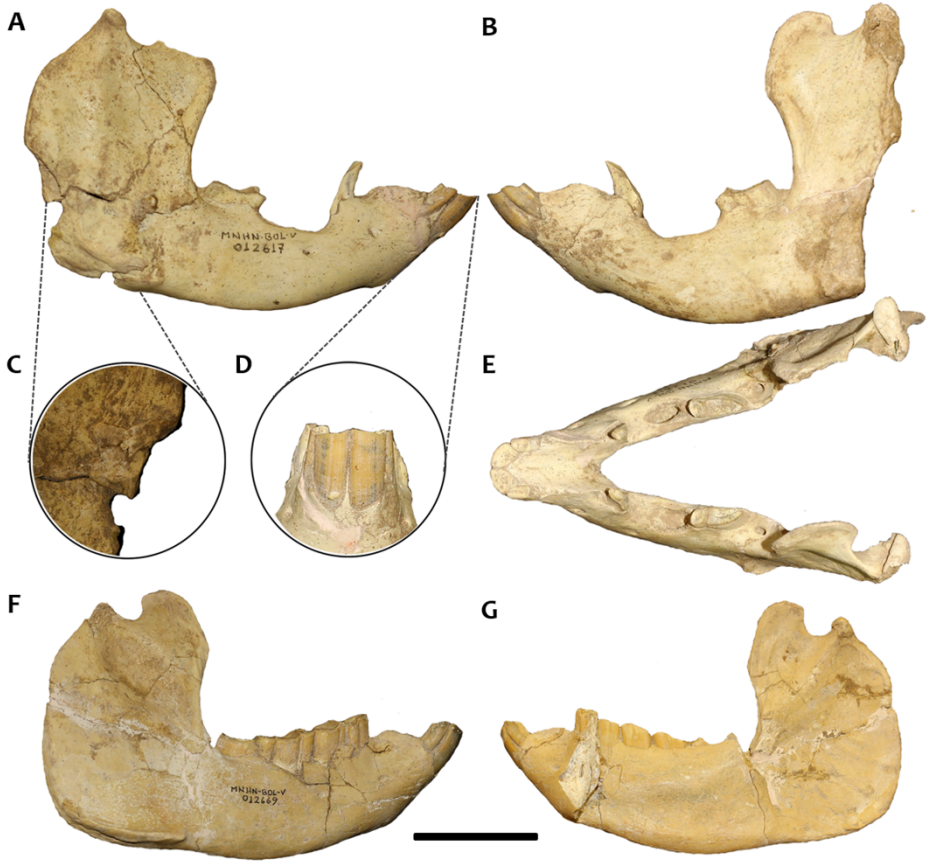

Figure 2 Supplementary material 1. Mandibles of *Plesiotypotherium achirense.* Pathological mandible (MNHN-Bol-V12617) (a-e) in lateral right (a); lateral left (b); detail of caudomedial border of the mandibular ramus (c); ventrorostral border (d); dorsal view (e). Non-pathological mandible (MNHN-Bol-V 12669) (f-g) in lateral right (f), medial views (g). Scale bar represents 5 cm (C and D are not to scale).

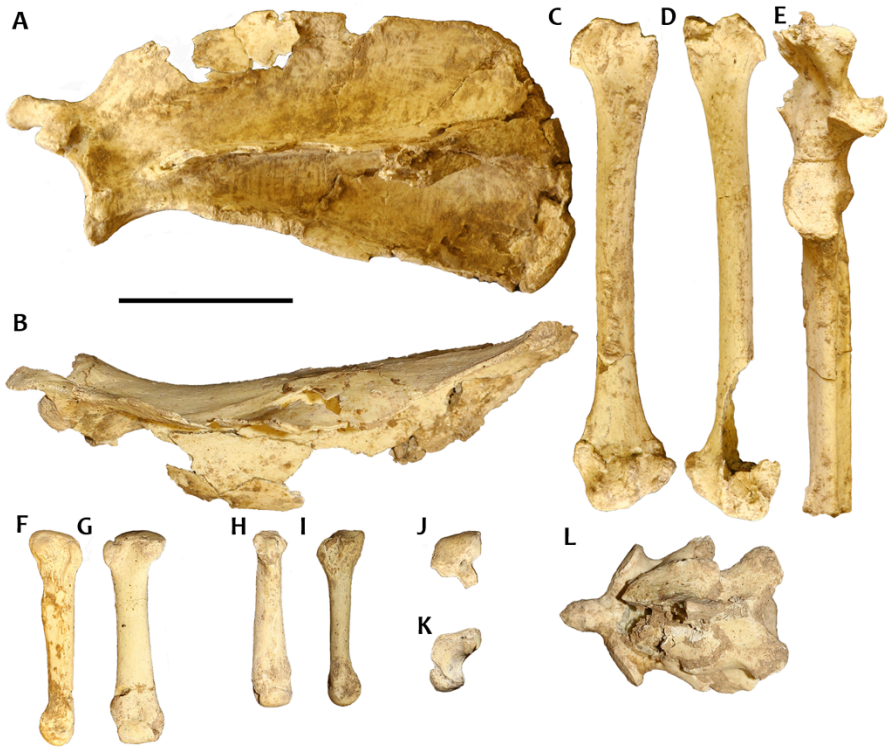

Figure 3 Supplementary material 1. Scapula, forelimb elements, axis and third cervical vertebra (C3) of *Plesiotypotherium achirense* (MNHN-Bol-V 12617). Left scapula in lateral and cranial views respectively (a,b); right radius in cranial view (c); left radius in cranial view (d); proximal epiphysis of left ulna (e); left Mc IV in medial and dorsal views respectively (f-g); right Mc V in dorsal and medial views respectively (h-i); left scaphoid in dorsal and distal views respectively (j-k); axis and third cervical vertebra (C3) in dorsal view (l). Scale bar represents 5 cm.

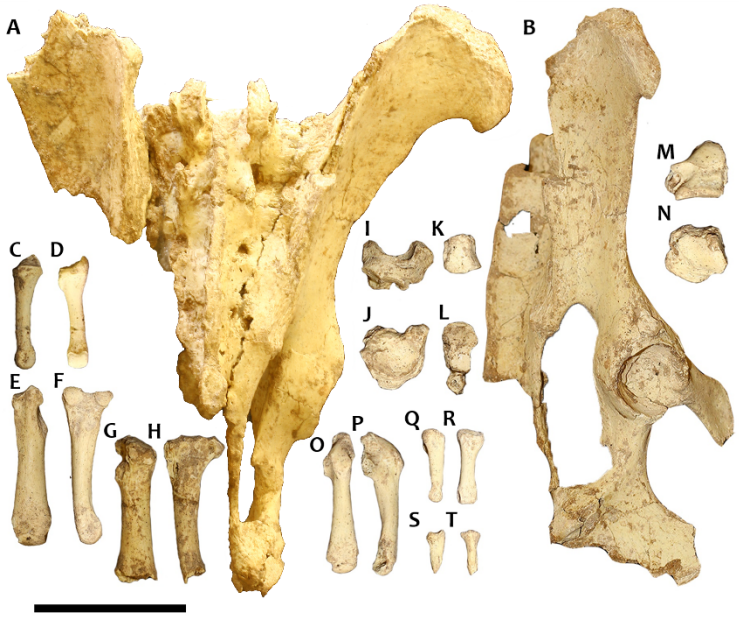

Figure 4 Supplementary material 1. Pelvis, sacrum, and hind limb of *Plesiotypotherium achirense* (MNHN-Bol-V 12617). Fused pelvis and sacrum in cranial and right lateral views respectively (a-b); left Mt I in medial and plantar views respectively (c-d); right Mt II in dorsal and medial views respectively (e-f); left Mt III in dorsal and medial views respectively(g-h); left navicular in dorsal and proximal views respectively (i-j); left ectocuneiform in dorsal and distal views respectively (k-l); left cuboid in dorsal and proximal views respectively (m-n); right Mt V in dorsal and lateral views respectively (o-p); second right phalanx of the digit V in lateral and dorsal views respectively (q-r); third right phalanx of the digit V in lateral and dorsal views respectively (s-t). Scale bar represents 5 cm. [prepared for page width]

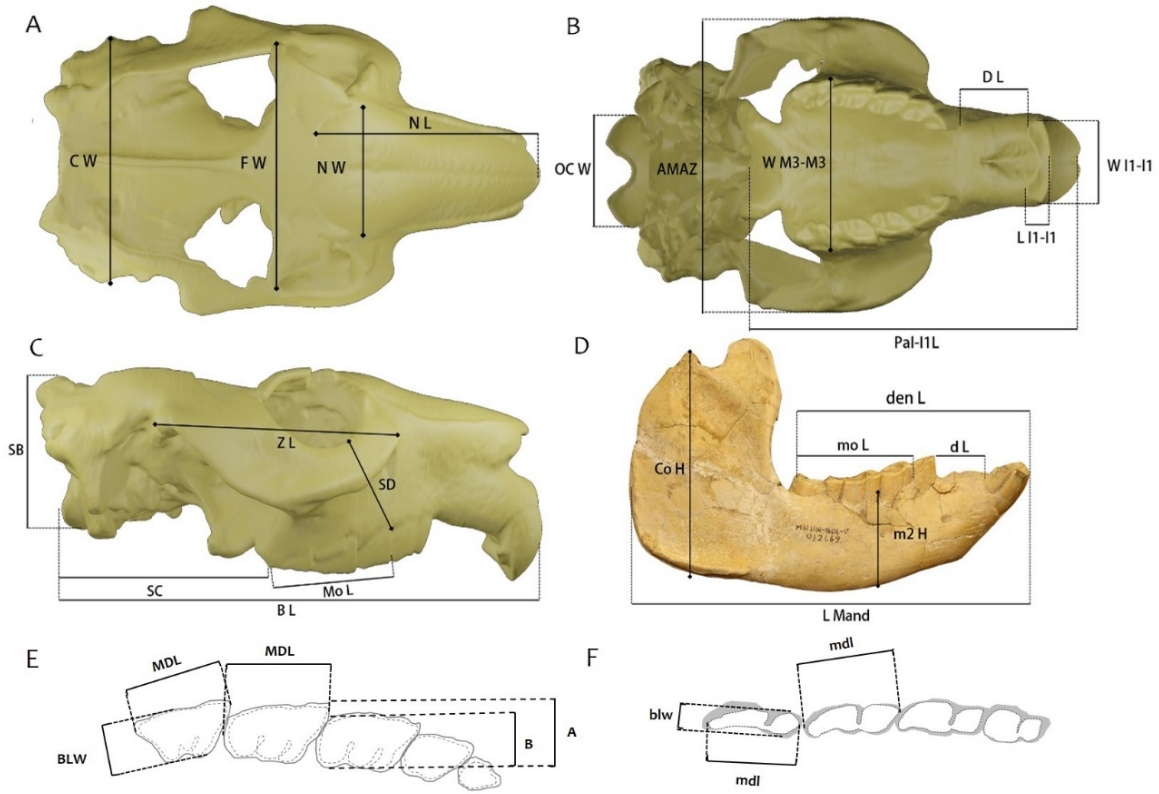

Figure 5 Supplementary material 1. Measurements for the cranial, mandibular and dental elements of *Plesiotypotherium achirense*. Skull in dorsal, ventral and lateral views, respectively (c-d); Mandible in lateral view (d); upper teeth in occlusal view (e); lower teeth in occlusal view (f).

Abbreviation	Description
N L	Nasal length
N W	Nasal width
F W	Maximal frontal width
C W	Maximal skull caudal width
BL	Basal skull length
Mo L	Upper molar series length
SC	Length of the posterior portion of the skull, measured from the occipital condyle to the distal m3 border
SB	Occipital height, measured from the base of the foramen magnum to the top of the occipital region
SD	Depth of the face under the orbit measured from the limit between molar and premolar tooth sequence to the nearest point of the orbit.
Z L	Maximal length of the zygomatic arch
L I1-I1	I1-I1 incisor length, measured from the rostral contact of both I1 to the caudal border between both I1
W I1-I1	I1-I1 incisor width
D L	Upper diastema length
W M3-M3	Width between the both M3 parastyles
AMAZ	Maximal width of the zygomatic arch
OC W	Occipital condyle width
Pal-I1 L	Maximal length of the palate to the labial border of the I1.
d L	Lower diastema length
mo L	Lower molar sequence length
den L	Lower dental length
m2 H	Mandibular body height at m2 level
Co H	Height of the mandibular condyle to the base of the mandibular ramus
Mand L	Mandibular length, measured from the caudal most border to the rostral most of the i1.

Table 1 Supplementary material 1. Description and summary of cranial and mandibular measurements (in mm) of *Plesiotypotherium achirense.*

Inventory number / Measurements	B L	Z L	D L	SC	Mo L	SB	AMAZ	N L	N W	F W	D L	W I1-I1	L I1-I1	W M3-M3	AMAZ	OC W
MNHN-Bol-V 12617		76.17			52.6	56	128.82	98.52	50	99.4	32.13	29	18	62.78	128.82	39.1
MNHN.F.ACH 26 (Holotype)	192	94.58	34	88	53.2	61	120.09	95.07	53	99.4	29.25	30	17	70.07	120.09	44.2
MNHN-Bol-V 8507	189	94.34	35	83	51.2	52	128.75	96.71	57	92.32	31.04	30	15	68.73	128.75	45.4
MNHN.F.ACH 23		90.88	38		53.1		125.5	98.18	50	92.46	25.69	32	17	74.48	125.5	
MNHN.F.ACH 63		85.26					121.66	85.76	47			26		73.97	121.66	
MNHN-Bol-V 12665		88.7	27	94	46.7	63		106.3	56	92.25	28.4	23	13			
MNHN-Bol-V 12664		80.16	31	76	39.3		106.36	76.54	47	79.85	25.96		11	56.64	106.36	

Table 2 Supplementary material 1. Skull measurements (in mm) of *Plesiotypotheirum achirense*. For abbreviations see Figure 5 Supplementary material 1.

Number	I1 MLD	I1BL W	P3 MDL	P3 BLW	P4 MDL	P4 BLW	M1 MDL	M1BL W	M2 MDL	M2 BLW	M3 MDL	M3 BLW	A	B	A/B
MNHN-Bol-V 12617	11.21	10.36	10.35	8.35	10.64	8.59	15.70	11.37	18.57	11.70	19.70	10.58			
MNHN.F.ACH 26 (Holotype)			10.04	8.53	11.51	10.35	16.08	11.55	18.16	11.62	19.67	10.91	11.9	9.66	1.23
MNHN-Bol-V 8507	18.08	10.255	10.3	6.87	8.01	10.23	15.88	11.43	17.02	11.28	18.81	10.08	12.55		
MNHN.F.ACH 33							14.88	12.08	16.63	11.8	19.55	11.14	11.64		
MNHN.F.ACH 28	18.845	10.17	9.15	8.47	10.18	10.34	17.52	10.15	18.89	11.29	20.21	10.79	12.49	9.65	1.29
MNHN.F.ACH 19	19.63	10.81	10.52	8.47	10.69	11.16	17.02	12.25	19.84	12.96	20.74	11.52	13.94	9.85	1.42
MNHN.F.ACH 39			10.52	8.37	10.35	11.97	17.95	11.325	17.685	11.145	19.365	10.445	11.15	9.41	1.18
MNHN.F.ACH 20	15.97	8.68	8.52	6.61	11.64	9.27	15.15	10.175	15.24	10.475	17.285	9.23	11.635	9.53	1.22
MNHN-Bol-V 12545	17.83	11.45	9.86	9.1	11.28	11.7	18.61	12.35	19.54	12.72	20.31	11.54	13.15		
MNHN-Bol-V 11999 (= ACH 355)					11.58	11.36	18.87	13.17	18.3	11.4	19.41	10.89		7.68	
MNHN-Bol-V 12665	14.08	8.685	7.23	8.19	8.68	9.43	15.56	10.19	17.64	10.16	16.38	9.56	10.58		
MNHN Bol V12664	11.59	7.28	4.61	5.89	7.36	7.63	12.81	9.09	13.89	9.21				8.79	
MNHN-Bol-V 11875 (=GB 228)			6.815	7.72	8.385	9.12	15.33	10.12	16.015	10.41	16.51	9.31	11	9.07	1.21
MNHN-Bol-V 11676	17.81	11.6	6.85	9.41	8.8	9.54	18.32	10.54	17.31	11.08	18.545	10.405	12.24		

Table 3 Supplementary material 1. Upper teeth measurements of *Plesiotypotherium achirense* (in mm). For abbreviations see Figure 5 Supplementary material 1.

Number	L Mand	mo L	den L	d L	Co H	m2 H
MNHN-Bol-V 12617	181.88	48.32	105.28	29.04	102.3	
MNHN-Bol-V 12663	164.35	43.46	90.82	20.79		36.095
MNHN-Bol-V 12670	176.54	53.58	105.96	21.18		42.38
MNHN-Bol-V 3330	174.57	52.45	101.34	18.92	106.46	33.405
MNHN-Bol-V 12669	171.27	49.885	99.58	20.56	95.72	39.085
MNHN-Bol-V 12670	174.4	56.76	104.99	20.505		42.055
MNHN-Bol-V 9880	210.65	59.74		24.79		42.615
MNHN.F.ACH 20	174.78	46.525	96.205	22.71		37.83
MNHN.F.ACH 26 (Holotype)	188.985	51.805	106.9	24.475	98.16	40.8
MNHN.F.ACH 17	180.78	54.99		21.1	107.88	41.96
MNHN.F.ACH 30		50.38				40.9
MNHN.F.ACH 29		47.02				36.36
MNHN.F.ACH 34		49.665				36.34
MNHN.F.ACH 32		54.98				41.89

Table 4 Supplementary material 1. Mandible measurements (in mm) of *Plesiotypotherium achirense.* For abbreviations see Figure 5 Supplementary material 1.

Number	i1 mdl	i1blw	i2 mdl	i2 blw	P4mld	p4blw	m1mld	m1blw	m2mld	m2blw	m3 MLD	m3 BLW
MNHN-Bol-V 12617	10.41	7.155	7.835	5.4	7.285	7.735					21.39	7.525
MNHN-Bol-V 12662	10.35	6.27			10.63	7.42	13.355	8.595	15.705	7.94	21.135	7.025
MNHN-Bol-V 12664					6.5	4.78	10.89	7.5	18.49	7.245		
MNHN-Bol-V 12663	8.855	5.315	5.765	4.3	8.74	6.055	11.965	7.715	13.275	7.375	18.775	6.58
MNHN-Bol-V 12641					7.64	5.71		5.35				
MNHN-Bol-V 12670	10.76	6.61	7.52	4.7	11.9	7.77	13.97	9.57	15.69	9.67		
MNHN-Bol-V 3330	10.99	6.655	5.15	4	10.38	6.75	13.955	8.33	16.045	7.22	19.28	7.1
MNHN-Bol-V 3334					11.66	6.92	13.55	8.45	14.81	7.63		
MNHN-Bol-V 3755					9.79	7.12	11.7	8.23				
MNHN-Bol-V 11677									13.24	8.04		
MNHN-Bol-V 12669	10.03	6.555	7.085	5	9.925	7.975	13.685	9.785	15.52	9.63	22.11	8.16
MNHN-Bol-V 12670	10.76	6.61	7.52	4.7	11.9	7.77	13.97	9.57	15.69	9.67		
MNHN-Bol-V 9880	12.11	7.47	8.44	4.9	11.935	8.385	16.23	10.09	17.23	9.53	23.64	9.37
MNHN-Bol-V 12642							13.08	7.85	12.22	7.24		
MNHN.F.ACH 20	9.1	5.775	6.41	4.3	9.93	6.815	12.76	8.445	15	8.155	19.76	7.02
MNHN.F.ACH 26	10.655	6.45	7.215	5.1	11.315	7.89	13.78	9.55	15.485	9.03	22.265	8.19
MNHN.F.ACH 17					11.215	7.665	14.73	9.43	15.94	8.98	23.165	7.49
MNHN.F.ACH 30												
MNHN.F.ACH 29	9.4	5.84	6.61	4.5	9.94	6.65	13.365	8.46	13.99	7.685	18.455	6.9
MNHN.F.ACH 36					12.26	8.69	15.59	9.97				

Table 5 Supplementary material 1. Lower teeth measurements (in mm) of *Plesiotypotherium achirense*. For abbreviations see Figure 5 Supplementary material 1.

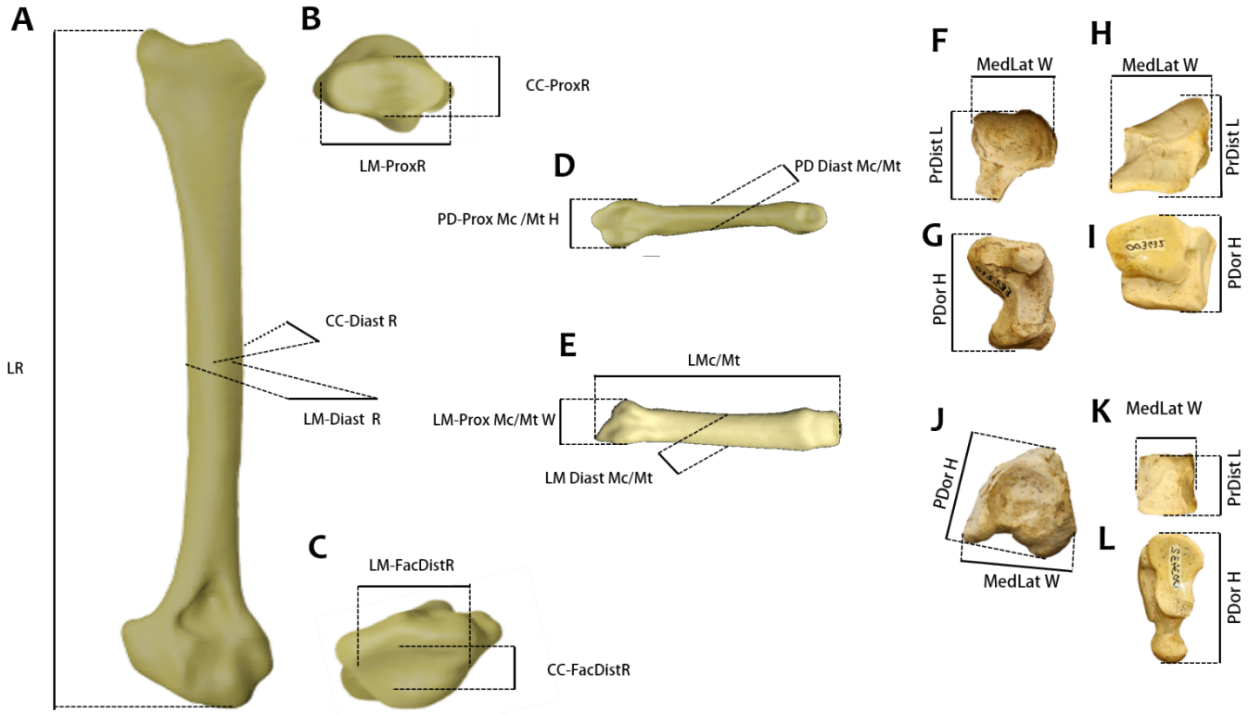

Table 6 Supplementary material 1. Measurements for postcranial elements (forelimb and hind limb). A-C. Radius measurements (a-c); Metacarpal or metatarsal measurements (d-e); Right scaphoid measurements in dorsal (f), and distal view (g); Left cuboid measurements in dorsal (H) and in distal view (i); Left navicular measurements in dorsal (h), and in proximal view (i); Left ectocuneiform measurements in dorsal (l), and in distal view (m).

Abbreviated measurement	Description for the measurement
LR	Radious length
CC-Diast R	Craniocaudal width of radius diaphysis
LM-Diast R	Lateromedial width of the radius diaphysis
CC-Prox R	Craniocaudal width of the radius head
LM-Prox R	Lateromedial width of the radius head
CC-Fac Dist R	Craniocaudal width of the fossa carpi radialis of radius
LM-Fac Dist R	Lateromedial width of the fossa carpi radialis of radius
LMc/Mt	Length of the Mc or Mt
LM-Prox W	Lateromedial width of the proximal epiphysis of the Mc or Mt
PD-Prox H	Plantodorsal width of the proximal epiphysis of the Mc or Mt
LM Diast Mc/Mt	Lateromedial width of the diastema of the Mc or Mt
PD-Diast Mc/Mt	Plantodorsal width of the diastema of the Mc or Mt
PrDist L	Proximodistal lenght (carpal or tarsal)
Med Lat W	Mediolateral width (carpal or tarsal)
P Dor H	Palmodorsal or plantodorsal height (carpal or tarsal)

Table 7 Supplementary material 1. Abbreviation, description and summary of postcranial measurements (in mm) of *Plesiotypotherium achirense*.

Number	Element	LR	CC-Diast R	LM-Diast R	CC-Prox R	LM-Prox R	CC-Fac Dist R	LM-Fac Dist R
MNHN-Bol-V 12617	Radius (R)	141.38	10.4	27.20	15.59	27.24	15.85	22.38
MNHN-Bol-V 12617	Radius (L)	142.08	10.6	27.34	15.11	27.34	14.5	21.08
MNHN-Bol-V 12760	Radius (R)	148.5	10.98		15.72	15.6	21.35	26.02
MNHN.F.ACH 18 (Paratype)	Radius	170.64	13.4		21.76	28.08	15.3	16.72

Table 8 Supplementary material 1. Radius measurements (in mm). For abbreviations see Table 7 Supplementary material 1.

Number	Element	LMc/Mt	LM-Prox Mc/Mt W	PD-Prox Mc/Mt H	LM Diast Mc/Mt	PD-Diast Mc/Mt
MNHN-Bol-V 12617	Mc V (R)	49.74	8.82	13.58	5.53	7.9
MNHN.F.ACH 34	Mc V (L)	54.89	9.19	13.78	7.76	5.73
MNHN-Bol-V 12617	Mc IV (L)	60.92	17.62	14.62	8.6	9
MNHN-Bol-V 3440	Mc IV (R)		18.4	16.1	10.4	8.9
MNHN-Bol-V 12617	Mt III (L)		13.82	20.99	9.17	7.73
MNHN.F.ACH 26 (Holotype)	Mt III (R)	57.39	12.77	20.21	9.99	7.8
MNHN-Bol-V 3336	Mt III (R)	59.58	13.09	19.94	9.83	8.3
MNHN-Bol-V 3738	Mt III (R)	57.2	15.3			
MNHN-Bol-V 3438	Mt III (L)		16	21.7	12.9	9
MNHN-Bol-V 12617	Mt V (L)	46.51	9.44	14.45	6.15	6.09
MNHN-Bol-V 12650	Mt V (R)	50.9	11.2	17.2	7.4	6.14
MNHN-Bol-V 3740	Mc V (R)	59.9	11.1	17.3	9.82	7.36

Table 8 Supplementary material 1. Measurements of the Mc or Mt. For abbreviations see Table 7 Supplementary material 1.

40Ar/39Ar dating

Samples were crushed and sieved and a 100–200 μm grain size was retained for feldspar separation. After magnetic separation, feldspar grains were selected under a stereomicroscope. The grains were leached with HNO3 (1N) for a few minutes and then repeatedly cleaned ultrasonically in distilled water and alcohol. Samples were packed in aluminium foil for irradiation in the core of the Triga Mark II nuclear reactor of Pavia (Italy) with several aliquots of the Taylor Creek sanidine standard (28.619 ± 0.034 Ma *in* Renne et al., 2011) as flux monitor. Argon isotopic interferences on K and Ca were determined by irradiation of KF and CaF_2 pure salts from which the following correction factors were obtained: $(^{40}Ar/^{39}Ar)$ K = 0.00969 ± 0.00038, $(^{38}Ar/^{39}Ar)$ K = 0.01297 ± 0.00045, $(^{39}Ar/^{37}Ar)$Ca = 0.0007474 ± 0.000021 and $(^{36}Ar/^{37}Ar)$Ca = 0.000288 ± 0.000016. $^{40}Ar/^{39}Ar$ step-heating analyses were performed at Géosciences Montpellier (France). The gas extraction and purification line consist of (a) an IR-CO_2 laser of 100 kHz used at 3-20% power to heat samples during 60 seconds, (b) a lenses system for beam focusing, (c) a steel chamber maintained at 10^{-8} - 10^{-9} bar, with a copper holder in which 2 mm-diameter blind holes were milled, and (d) two Zr-Al getters for purification of gases. Argon isotopes are analysed with an Argus VI multi-collection mass spectrometre (with 4 faradays for masses ^{40}Ar-^{37}Ar and ion counting on ^{36}Ar). One minute was allowed for equilibration before analysis. Mass discrimination of machines is followed daily. Mass discrimination was monitored daily using an automated air pipette and provided a mean value of 0.99985 ± 0.00274 per dalton. Micropopulations of feldspar crystals were distributed in holes of the copper holder and were step heated. Blank analyses were performed every three sample analyses. Raw data of each step and blank were processed and ages were calculated using the ArArCALC-software (*Koppers*, 2002). Isotopic ratios were corrected for irradiation interferences and air contamination using a mean air value $(^{40}Ar/^{36}Ar)_{atm}$ of 298.56 ± 0.31

(Lee et al., 2006; Renne et al., 2009). Ages are statistically analysed in two ways: ^{39}Ar released spectra and inverse isochrones. Plateau ages are calculated from at least three consecutive ^{39}Ar release steps comprising up to 50% of total $^{39}Ar_K$ released and overlapping at the 2σ confidence level (Fleck et al., 1977). Isochrone ages are accepted when mean square weighted deviation (MSWD) is close to 1 and the $^{40}Ar/^{36}Ar$ intercept within 2σ from the $(^{40}Ar/^{36}Ar)_{atm}$ value. The analytical data are reported in the tables ACH TUF 4A A9.detailed.xls, ACH TUF 3A A10 plateau.detailed.xls and ACH TUF 3A A10 isochrone.detailed.xls. All errors are quoted at the 2σ level uncertainty including the error on the irradiation factor J.

Fleck, R.J., J. F. Sutter, and D. H. Elliot. 1977. Interpretation of discordant 40Ar/39Ar age-spectra of mesozoic tholeiites from Antarctica: Geochimica et Cosmochimica Acta 41: 15–32.

Lee J-Y, K. Marti, J. P. Severinghaus, K. Kawamura, H. S. Yoo, J. B. Lee, and J. S. Kim. 2006. A redetermination of the isotopic abundances of atmospheric Ar: Geochimica et Cosmochimica Acta 70:4507–4512.

Renne, P.R., G. Balco, K. R. Ludwig, R. Mundil, and K. Min. 2011. Response to the comment by W.H. Schwarz et al. on "Joint determination of 40K decay constants and 40Ar*/40K for the Fish Canyon sanidine standard, and improved accuracy for 40Ar/39Ar geochronology" by P.R. Renne et al. (2010): Geochimica et Cosmochimica Acta 75:5097–5100.

Renne, P.R., W. S. Cassata, and L. E. Morgan. 2009. The isotopic composition of atmospheric argon and 40Ar/39Ar geochronology: time for a change: Quaternary Geochronology 4:288-298.